Photoacoustics 34 (2023) 100565

Contents lists available at ScienceDirect

Photoacoustics

journal homepage: www.elsevier.com/locate/pacs

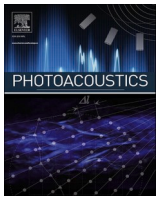

Ultrafast magnetoacoustics in Galfenol nanostructures

A.V. Scherbakov [a,*], T.L. Linnik [a,b], S.M. Kukhtaruk [b], D.R. Yakovlev [a], A. Nadzeyka [c], A.W. Rushforth [d], A.V. Akimov [d], M. Bayer [a]

[a] Experimentelle Physik 2, Technische Universität Dortmund, 44227 Dortmund, Germany
[b] Department of Theoretical Physics, V.E. Lashkaryov Institute of Semiconductor Physics, 03028 Kyiv, Ukraine
[c] Raith GmbH, 44263 Dortmund, Germany
[d] School of Physics and Astronomy, University of Nottingham, Nottingham NG7 2RD, United Kingdom

ARTICLE INFO

Keywords:
Laser Ultrasonics
Acoustic phonons
Magnons
Magnetic nanostructures
Magnonphonon interaction
Phonon guiding

ABSTRACT

Phonons and magnons are prospective information carriers to substitute the transfer of charge in nanoscale communication devices. Our ability to manipulate them at the nanoscale and with ultimate speed is examined by ultrafast acoustics and femtosecond optomagnetism, which use ultrashort laser pulses for generation and detection of the corresponding coherent excitations. Ultrafast magnetoacoustics merges these research directions and focuses on the interaction of optically generated coherent phonons and magnons. In this review, we present ultrafast magnetoacoustic experiments with nanostructures based on the alloy (Fe,Ga) known as Galfenol. We demonstrate how broad we can manipulate the magnetic response on an optical excitation by controlling the spectrum of generated coherent phonons and their interaction with magnons. Resonant phonon pumping of magnons, formation of magnon polarons, driving of a magnetization wave by a guided phonon wavepacket are demonstrated. The presented experimental results have great application potential in emerging areas of modern nanoelectronics.

1. Introduction

The high demand of modern nanoelectronics in energy-effective solutions stimulates the search for new information carriers, where coherent phonons and magnons are promising charge-free alternatives. Magnon-phonon interaction enables sharing their main advantages: collective excitation with the robustness of phonons and tunability of magnons operated up to THz frequencies could be a game-changer. This is the focus of ultrafast magnetoacoustics, which exploits ultrafast optical excitation of a magnetic material to generate and detect coherent phonons and magnons. It can be considered a combination of two independent research fields exploiting ultrashort laser pulses: picosecond ultrasonics [1] and ultrafast (i.e. femtosecond) optomagnetism [2,3]. The first field was started in 1984 by Humphrey Maris et al. [4] with an experiment on generating coherent acoustic (phonon) wavepackets in thin films of a-As_2Te_3. It has been quickly extended to a wide range of materials, including ferromagnetic metals, e.g. Nickel [5,6]. Nickel is one of three natural metallic ferromagnets (along with Iron and Cobalt), but the laser-induced modulation of magnetic properties was not studied in the first ultrafast acoustic experiments. It was addressed only ten years later by Jean-Yves Bigot in the first experiment on ultrafast laser-induced demagnetization of Ni [7]. This breakthrough study launched ultrafast optomagnetism. In 2002, van Kampen et al. showed that ultrafast modulation of the net magnetization of a Ni film generates a wavepacket of coherent magnons, i.e., spin waves [8].

The wavelength of phonons and magnons generated by the laser pulse is set by the spatial profile of the light field in the excited material. In the direction normal to the excited surface, it is governed by the penetration depth of light, i.e., about 10 nm in metals. Along the plane surface it is set by the size of the focused laser spot, which is limited by the optical excitation wavelength and can be as small as on the order of 100 nm. From the diagram shown in Fig. 1a, one can see that for this range of wavelengths, the characteristic frequencies of phonons and magnons overlap. Thus, the condition of magnon-phonon resonance [9,10], namely matching both their wavevectors and frequencies, are naturally fulfilled. However, despite this coincidence and the same material used in the first experiments, ultrafast acoustics and optomagnetism had been remaining “uncoupled” for quite a long time.

The two research fields have merged in 2010 in experiments with the ferromagnetic semiconductor (Ga,Mn)As [11]. In this study, an optically

* Corresponding author.
E-mail address: alexey.shcherbakov@tu-dortmund.de (A.V. Scherbakov).

https://doi.org/10.1016/j.pacs.2023.100565
Received 4 August 2023; Received in revised form 23 October 2023; Accepted 23 October 2023
Available online 26 October 2023

generated coherent phonon wavepacket injected into a $Ga_{0.95}Mn_{0.05}As$ film from the substrate excited precession of the magnetization, i.e., a coherent superposition of the magnon modes [12]. The amplitude of precession was large enough for its time-resolved optical detection. Subsequent experiments with Ni films demonstrated the excitation of coherent magnons by coherent phonons generated directly in a ferromagnetic material [13]. This work defined a new research field, which was developed experimentally [14–25] and theoretically [26–35] over the next decade.

A number of magnetoacoustic effects, such as resonant excitation of coherent magnons by phonons and vice versa, propagation and attenuation of elastic waves in magnetized media, formation of hybridized magnetoelastic waves, were theoretically predicted in the 50ies of the 20th century [9,10]. These effects were experimentally observed in bulk ferrimagnetic garnets [36,37], where extremely low phonon and magnon decay rates made the strong magnon-phonon coupling detectable by the experimental techniques that were available at that time. However, in the case of higher magnon frequencies and much faster decay rates, the magnon-phonon interaction is hardly trackable for conventional experimental methods based on piezoelectric generation and detection of acoustic waves. Ultrafast magnetoacoustics considerably pushes the research borders: ultrafast optical excitation and direct time-resolved detection of the phonon and magnon transients made the effects governed by magnon-phonon interaction detectable at sub-THz frequencies and at spatial scales down to several atomic layers, to provide new insights into magnon-phonon interaction.

Besides the apparent research interest, a growing number of ultrafast magnetoacoustic experiments has been stimulated by several application areas, which are looking for new approaches to overcome their specific problems. First, magnetic recording, which remains the most reliable and cheapest way to store information, has reached a speed limit [38] and requires new ultrafast tools to control magnetic order. In the last ten years, phonon-induced and phonon-assisted magnetization switching has made gigantic steps from theoretical models [27,32,39] to breakthrough experiments [40]. Second, information technologies have encountered the problem of rapidly increasing power consumption for the rapidly growing amounts of processed information. This has stimulated the active search for data carriers that do not involve charge transport [41,42]. Both magnons and phonons are among the considered alternatives [43–45], and their interaction with the formation of a hybridized state (i.e., a magnon polaron) is the way to combine their main advantages and minimize their drawbacks [46]. Magnon-phonon hybridization is also attractive for quantum communications for manipulating excitations at the quantum level [47,48].

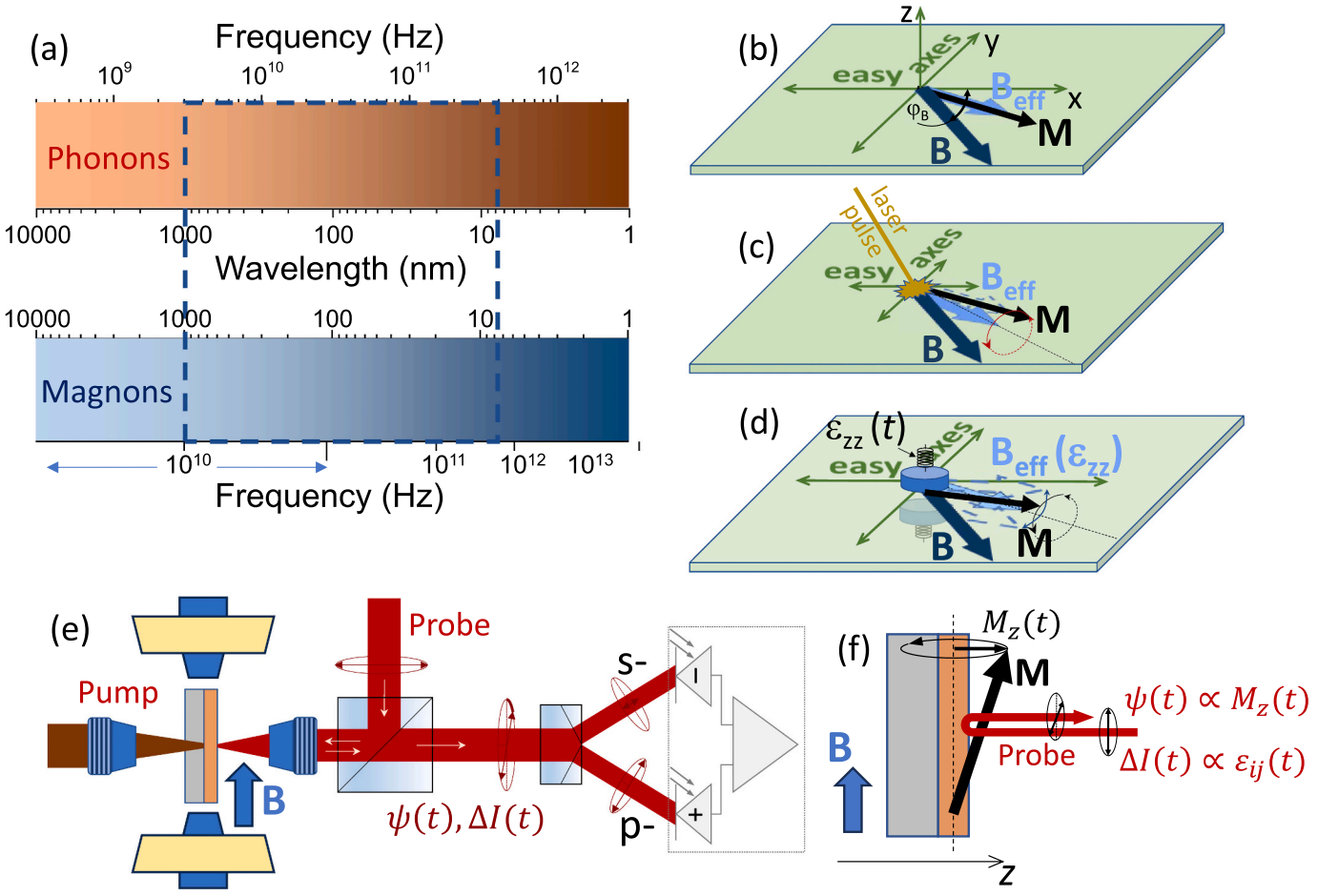

Fig. 1. Excitation and detection of coherent magnons and phonons in a metallic ferromagnet. (a) Frequencies and wavelengths of phonons and magnons in ferromagnetic metals. The dashed frame shows the typical range of frequencies and wavelengths excited by a femtosecond laser pulse in a ferromagnetic metal. (b)-(d) Used coordinate system and excitation of the magnetization precession: (b) equilibrium state with the magnetization, **M**, along the effective field, $\mathbf{B}_{\mathbf{eff}}$, defined by the balance of the external magnetic field, **B**, and the anisotropy field, which defines the easy axes of magnetization; (c) ultrafast tilt of $\mathbf{B}_{\mathbf{eff}}$ due to the rapid decrease of the anisotropy field, induced by the femtosecond laser pulse, followed by precession of **M**; (d) phonon-induced precession by a quasi-harmonic modulation of $\mathbf{B}_{\mathbf{eff}}$ via dynamical strain. (e) Experimental scheme, in which a metallic ferromagnetic film is excited from the backside through the transparent substrate. The transient Kerr rotation and reflectivity signals, $\psi(t)$ and $\Delta I(t)$, given by the z-projection of the precessing magnetization and the dynamical strain, respectively, as illustrated in (f). The signals are measured by a balanced photoreceiver as the difference $[\psi(t)]$ and the sum $[\Delta I(t)]$ of the intensities of the pulses of orthogonal polarizations, split from the linearly polarized probe pulse by a Wollaston prism.

The range of materials studied by ultrafast magnetoacoustic experiments is not so wide. It includes the well-studied Ni [13,16–18,25], Yttrium-Iron Garnets (YIG) [19–21], alloys like (Ga,Mn)As [10,11] and Terfenol-D [23], and multilayer structures [22]. The present review focuses on ultrafast magnetoacoustic experiments with epitaxial films of the metallic ferromagnetic alloy of Iron and Gallium known as Galfenol [49]. Among other magnetic materials, Galfenol stands out due to the beneficial combination of its properties. It is characterized by an Iron-like large saturation magnetization and a high Curie temperature, a narrow magnon resonances, and an enhanced magnetoelastic coupling. Moreover, this material is technology-friendly: thin Galfenol films can be epitaxially grown on semiconductor substrates and patterned by post-growth lithography with preserved cubic crystal structure and the corresponding magnetic anisotropy [50,51]. It allows fine-tuning of the magnon modes' dispersion, their response to optical excitation, and their interaction with coherent phonons. The present review illustrates manifestations of this unique combination in several ultrafast magnetoacoustic experiments.

The review is structured as follows. First, in Section 2 we present the basics of the ultrafast magnetoacoustics experiment. In Section 3, we show the magnon response on the ultrafast optical excitation in Galfenol films of varied thicknesses to illustrate its essential characteristics. In Section 4, we demonstrate the coherent driving of magnons by phonons localized in a plane phononic Fabry-Perot nanoresonator. Section 5 presents the direct observation of the strong magnon-phonon coupling in a patterned Galfenol film. The formation of the hybridized excitation known as magnon polaron is revealed. In Section 6, we show the driving of magnons by a guided multimode phonon wavepacket. Prospective directions of further research are discussed in the conclusion.

2. Ultrafast magnetoacoustic experiments with Galfenol films

2.1. Qualitative consideration

In the experiments presented in this review the studied sample consists of a thin plain or patterned film of Galfenol deposited on a nonmagnetic substrate. The film is excited by femtosecond laser pulses, which generate coherent phonons and magnons simultaneously. The generation of coherent acoustic phonons is the result of ultrafast thermal expansion [5]. The generated coherent phonon wavepacket spectrum contains frequencies up to about 100 GHz and depends on the thickness of the film.

The generation of coherent magnons is based on two mechanisms: the optically-induced modulation of the magnetic anisotropy [8,52] and phonon-induced strain through inverse magnetostriction [14,51]. Both mechanisms can be described by the Landau-Lifshitz-Gilbert equation for the magnetization, **M**, precessing around the time-dependent effective magnetic field, $\mathbf{B}_{\text{eff}}$ [53]:

$$\frac{d\mathbf{m}}{dt} = -\gamma\left[\mathbf{m}\times(\mathbf{B}_{\text{eff}}(t)+D\nabla^2\mathbf{m})\right]+\alpha\left[\mathbf{m}\times\frac{d\mathbf{m}}{dt}\right]. \quad (1)$$

Here $\mathbf{m}=\mathbf{M}/M_0$ is the normalized magnetization vector ($M_0$is the saturation magnetization), γ is the gyromagnetic ratio, D is the exchange spin stiffness, and α is the Gilbert damping coefficient. The effective field $\mathbf{B}_{\text{eff}}(t) = -\nabla_{\text{m}}F_{\text{m}}$, where F_{m} is the normalized free energy density. For the case of a thin plain film, $F_{\mathbf{m}}$ can be written as:

$$F_m(m,t) = -m\cdot B + B_d m_z^2 + B_1(m_x^2m_y^2 + m_x^2m_z^2 + m_y^2m_z^2) + B_u m_x m_y$$
$$+b_1\sum_i \varepsilon_{ii}m_i^2 + b_2\sum_{i,j}\varepsilon_{ij}m_im_j + 2b_4\sum_{i,j,l}\varepsilon_{ii}m_j^2m_l^2 + ., \quad (2)$$

where $i,j,l = x,y,z$, and the coordinate axes correspond to the main crystallographic directions (z is parallel to the film normal). The first term in Eq. (2) describes the interaction of the magnetization with the external magnetic field, **B**; the second term sets the shape anisotropy, which in the case of a plain film is given by the demagnetizing field $B_d = \mu_0 M_0/2$ (μ_0 is the permeability) holding the magnetization in the film plane; the third and fourth terms represent the cubic and uniaxial anisotropy fields, B_1 and B_u, which determine the in-plane direction of the easy axes of magnetization. The uniaxial anisotropy deviates the easy magnetization axes from the main crystallographic directions toward the [110]-direction and makes the hard magnetization axes [110] and $[1\bar{1}0]$ non-equivalent. The three following terms describe the interaction of the magnetization with the phonon-induced dynamical strain, $\varepsilon_{ij}\quad(i,j=x,y,z)$, which efficiency is determined by the magnetoelastic coefficients, b_1, b_2, b_4. (the coefficients of higher orders are omitted).

Fig. 1b – d illustrate the generation of coherent magnons through the modulation of the effective field showing also the coordinate system used below. At equilibrium, $\mathbf{M} \parallel \mathbf{B}_{\text{eff}}$, and this direction corresponds to the minimum of the free energy set by the balance of the external magnetic field and the anisotropy fields. The femtosecond optical excitation instantly decreases the anisotropy fields due to ultrafast demagnetization and lattice heating [8,52]. The tilt of $\mathbf{B}_{\text{eff}}$ toward **B** launches the precession of **M** as shown in Fig. 1c, and its following decay is defined by the Gilbert coefficient, α. The excitation of magnons by coherent phonons also occurs through the modulation of $\mathbf{B}_{\text{eff}}$. The effect of a picosecond strain pulse, which duration is much shorter than the period of precession, may also be considered as a quick tilt of $\mathbf{B}_{\text{eff}}$ launching the precessional response of **M** [13,26]. The localized phonon modes induce a periodic modulation of $\mathbf{B}_{\text{eff}}$ at the corresponding frequencies with a decay rate set by the phonon mode lifetime (Fig. 1d). The precessional response of **M** is a superposition of the Eigen magnon modes of the ferromagnetic nanostructure [8,12]. Their spatial profiles and spectral positions are defined by the structural design, which determines the spatial profile of the demagnetizing field, the boundary conditions and the spin stiffness. The amplitude of a specific magnon mode in the coherent magnon wavepacket is determined by its spatial overlap with the spectral component of the corresponding excitation (at the frequency of the magnon mode) and its spectral amplitude [12]. Since the direction of **M**, the special profiles, and spectral positions of the magnon modes can be tuned by the external magnetic field, it becomes possible to realize a specific excitation mechanism or to couple selected magnon and phonon modes of the studied structure [12]. This selectivity will be demonstrated in the experiments presented in Sections 3–5.

It is worth to mention that the energy transfer from magnons to phonons, i.e., the generation of coherent phonons by the precessing magnetization through direct magnetostriction is possible. This mechanism of excitation was shown in a number of microwave experiments [36,37]. However, in the case of direct ultrafast optical excitation of a ferromagnetic metal, the energy pumped directly to coherent phonons is significantly larger than the energy flow mediated by coherent magnons. Thus, in most ultrafast magnetoacoustic experiments, the magnon-phonon interaction is studied by monitoring the magnon response. Under certain conditions, such as magnon-phonon resonance, the contribution from coherent phonons dominates over direct optical excitation in the coherent magnon response.

2.2. Experimental setup

The experiments presented in the present review were carried out using the pump-probe technique schematically shown in Fig. 1e and f. The femtosecond pump pulses of about 100 fs duration excite the Galfenol film at its frontside or at the backside transmitted through the substrate, which is transparent at the wavelength of the pump pulses (the scheme shows the latter case). The typical pump fluence applied is between 0.1 and 10 mJ/cm^2. The linearly polarized probe pulses focused on the front surface serves for time-resolved detection of the transient phonon and magnon signals. The phonon signal is measured by monitoring the modulation of the reflected probe pulse intensity, ΔI,

governed by the photoelastic effect [4]. The magnon response is measured by monitoring the rotation of the probe polarization plane, ψ, caused by the polar magneto-optical Kerr rotation (KR) and proportional to the normal projection of the macroscopic magnetization, M_z [54]. The signals are measured in a differential scheme using a balanced photodetector with sub-ps time resolution provided by a variable time delay between the probe and pump pulses. Two schemes based on two alternative laser systems were used for the measurements. In the first scheme, the pump and probe pulses are split from the pulses generated by a regenerative amplifier (RegA) with a 100-kHz repetition rate. In this scheme, the variable delay was provided by a 1-m mechanical delay line. The modulation of the pump pulses by a chopper at the frequency of ~1 kHz with synchronous detection of the transient signals by a lock-in amplifier was used to eliminate broadband noise and achieve the desired signal-to-noise ratio. In the second scheme, we use a technique known as asynchronous optical sampling (ASOPS) [55] based on two mode-locked Erbium-doped ring-fiber laser oscillators (TOPTICA FemtoFiber Ultra 1050 and FemtoFiber Ultra 780) with a repetition rate of 80 MHz. The variable delay was realized using an 800-Hz offset of the oscillators' repetition rates. In contrast to the scheme with a mechanical delay line, in the ASOPS scheme the desired signal-to-noise ratio was achieved by accumulating and averaging of the transient signals in the full time window without modulation of the pump or probe pulses.

All the experiments in this review were carried out with $Fe_{0.81}Ga_{0.19}$ films epitaxially grown on (100)-GaAs substrates and covered by a protective Aluminium or Cromium layer of 2 nm. The lateral patterning of the films was made using focused Ga-ion beam (FIB) milling (Raith VELION FIB-SEM). The main parameters of the films obtained from the literature [49,56–58] and by fits of the experimental signals are the following: $M_0 = 1.6 - 1.8$ T, $B_1 = 20 - 30$ mT, $B_u = 4 - 10$ mT, $b_1 = b_2 = -7$ T, $b_4 = 1$ T, $\alpha = 0.006 - 0.008$. The external magnetic field was always applied in the film plane. Before every measurement, the films were magnetized into single domain state. The main measurements were done for ambient conditions at room temperature.

3. Optical excitation of magnon modes in Galfenol nanolayers

First, we consider the experiment [59] in which the optical excitation of magnetization precession is dominant and the contribution of coherent phonons is negligible. The structures studied in this experiment are $Fe_{0.81}Ga_{0.19}$ films with thicknesses, h, between 4 and 120 nm. The experiment was carried out using the ASOPS scheme in the experimental geometry shown in Fig. 2a. For in-plane orientation of $\mathbf{M}$ ($m_z = 0$), the demagnetization and the corresponding decrease of B_d do not contribute to the modulation of $\mathbf{B}_{\mathbf{eff}}$, and the optically induced modulation of $\mathbf{M}$ occurs through the temperature-dependence of the cubic and uniaxial anisotropy fields. The pump spot diameter (10 μm in the present experiment) is significantly larger than the penetration depth of the laser pulse and the generated picosecond strain pulse is purely longitudinal, so that the only strain component ε_{zz} is excited. Its contribution to the modulation of $\mathbf{B}_{\text{eff}}$ through the second-order term [the last term in Eq. (2)] is significantly weaker than the optically-induced modulation of B_1

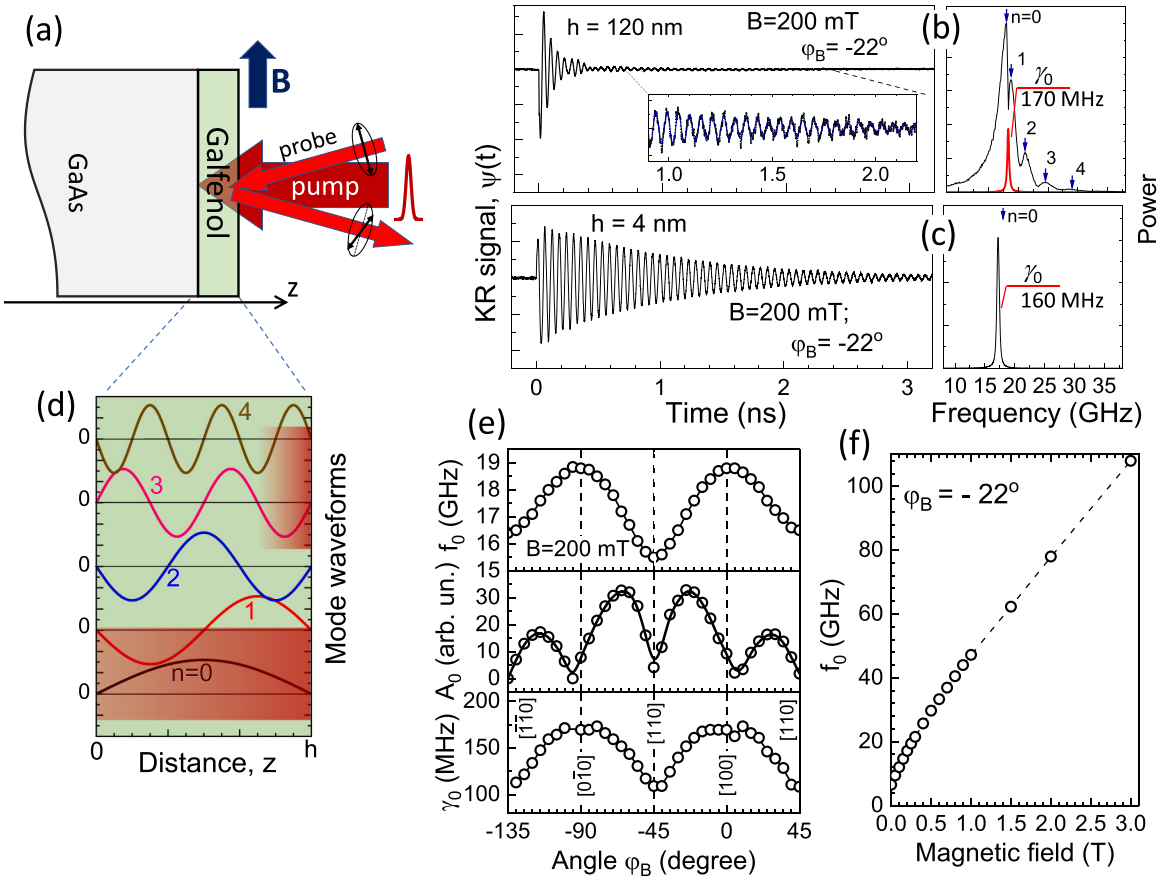

Fig. 2. Optical excitation of multi- and single –mode precession in thin $Fe_{0.81}Ga_{0.19}$ films [59]. (a) Experimental scheme. (b),(c) Transient Kerr rotation (KR) signals measured in films of 120-nm (b) and 4-nm (c) thickness (left panels) and their FFTs (right panels). The inset in the left panel of (b) shows the zoomed section of the signal with the monochromatic contribution of the fundamental magnon mode (n = 0). The sole contribution of the fundamental modes is confirmed by the FFT calculated in the time window between 1 and 8 ns and shown by the red curve in the right panel, in comparison with the FFT calculated in the whole measured time range. (d) The waveform of the quantized exchange magnon modes in a film of thickness h for pinned boundary conditions. The red rectangles schematically illustrate the distribution of the optical excitation along the film depth in the 4-nm (lower rectangle) and 120-nm samples (upper rectangle). (e), (f) Dependences of the frequency, f_0, amplitude, A_0, and decay rate, γ_0, of the KR signal measured in the 4-nm film on direction (e) and strength (f) of the external magnetic field, $\mathbf{B}$.

and B_u and may be neglected [52].

Fig. 2b and c show the KR signal, $\psi(t)$, measured in the 120-nm and 4-nm films at $B = 200$ mT applied at the azimuthal angle $\varphi_B = -22°$. The signal measured in the thick film is characterized by a fast decay, and its fast Fourier transform (FFT) shown in the right panel has a broad spectrum in which several spectral lines are resolved. These spectral peaks correspond to the exchange magnon modes quantized along the film normal, which spatial profiles for the pinned boundary conditions [60] are shown in Fig. 2d. The spectral splitting between the modes has a quadratic dependence on the mode number: $f_n - f_0 \propto \frac{2\pi}{h} D n^2$, where n is the mode number ($n = 0, 1, 2...$). The value $D = 1.5 \times 10^{-17}$ Tm^2 obtained from the fit of the experimental data agrees well with the values measured in ferromagnetic resonance (FMR) experiments [61]. The fast decay of $\psi(t)$, which is typical for metallic ferromagnets like Co or Ni, is due to the rapid damping of the high-order modes. The lifetime of the fundamental magnon (FM) mode ($n = 0$), τ_0, exceeds 1 ns and the FM mode solely contributes to $\psi(t)$ at $t > 1$ns. The FFT calculated for the time window between $1 < t < 10$ ns (shown by the dashed red curve in the right panel) contains a single spectral line. It is slightly shifted to higher frequencies due to lower temperature of the Galfenol film relatively to the earlier time interval. Its decay rate of $\gamma_0 = 1/2\pi\tau_0 = 170$ MGz corresponds to the Gilbert damping $\alpha = 0.006$, which agrees with the damping rate obtained in FMR experiments [51,61]. The KR signal measured in the thinnest film of 4-nm thickness for the same experimental conditions is shown in Fig. 2c. It shows harmonic oscillations with single frequency, and its power spectrum has a single line of Lorentzian shape. The frequency and decay rate correspond to the FM mode. KR signals characterized by single precession frequencies were also measured in films with $h = 5$, 10 and 20 nm thickness.

The presence of the high-order magnon modes in the film with $h = 120$ nm and their absence in the films with $h \leq 20$ nm are explained by the spatial profile of the optically-induced modulation of $\mathbf{B}_{\text{eff}}$ along the z-axis. The modulation of the effective field occurs on the time scale of about 1 ps set by the thermalization of hot electrons generated by the laser pulse. This excitation has a broad spectrum with frequencies up to 1 THz and covers the frequency range for high-order modes for the films with all studied thicknesses. However the relative spatial distribution of $\mathbf{B}_{\text{eff}}$ across the film, which is set by the penetration depth of the pump pulse $\eta \approx 20$ nm as illustrated in Fig. 2d, depends on h. The efficiency of magnon mode excitation depends on the spatial overlap between $\mathbf{B}_{\text{eff}}$ and magnon modes. In 120-nm film, the excitation is strongly nonuniform, resulting in quite efficient excitation of high-energy magnon modes [8]. The excitation efficiency decreases with the increase of n, as clearly observed in Fig. 2c: the spectral amplitude of the magnon spectral line decreases by more than one order of magnitude with n increasing from 0 to 4, while their spectral splitting is significantly smaller than the excitation spectrum. In 4-nm film, where the boundary conditions for the magnon modes become free-like [62], the pump excitation is uniform and its overlap with the high-order modes (both even and odd ones) is negligibly small. Thus, only the fundamental magnon mode ($n = 0$) is excited.

The sole contribution of the FM-mode to the KR signal in thin films allows careful measurements of the dependence of its main characteristics on the external magnetic field. Fig. 2e and f show the dependences of the frequency, f_0, spectral amplitude, A_0, and the decay rate, γ_0, on the direction and strength of $\mathbf{B}$. The measured dependences correspond to cubic anisotropy with a small uniaxial distortion. The highest frequency is measured with $\mathbf{B}$ applied along the easy axes, which are slightly inclined from the [100] and [010] crystallographic directions. The signals measured at $\mathbf{B}$ along the [110] and [1$\bar{1}$0] directions, which are the hard (but non-equivalent) axes, possess the smallest decay rates of $\gamma_0 = 100$ MHz, which corresponds to the lifetime $\tau_0 = 1.6$ ns. The dependence $f_0(B)$ is almost linear and reaches sub-THz frequencies.

The demonstrated results are the most important magnon properties of Galfenol. The magneto-crystalline anisotropy enables selection of the mechanism responsible for the excitation of coherent magnons by choosing direction and strength of the external magnetic field and allows tuning of the magnon frequencies across a wide range. This tunability is combined with small magnon decay rates, which make the spectrally close magnon modes well resolvable in the spectrum of the optically generated magnetization precession. The following experiments illustrate the advantages of this combination for ultrafast magnetoacoustics.

4. Resonant phonon driving of the magnetization precession

In a conventional FMR experiment, the precessional motion of the magnetization is driven by an ac- magnetic field generated by a microwave source. An alternative way of driving is harmonic modulation of the effective field by the phonon-induced strain as discussed in Section 2 and illustrated in Fig. 1d. If a ferromagnetic nanostructure hosts a long-living phonon mode, which can be excited by a femtosecond laser pulse, the magnon response to the optical excitation will be mediated by monochromatic coherent phonons through the phonon-induced harmonic strain. The experiment presented in this section illustrates this effect [63].

The structure studied in the next experiment is shown in Fig. 3a. In comparison with the previous study, the difference is the presence of two superlattices (SLs) deposited between the GaAs substrate and the $Fe_{0.81}Ga_{0.19}$ film of 69-nm thickness. Both SLs contain 10 pairs of GaAs/AlAs bilayers with the thicknesses 59/72 nm (SL1) and 42/49 nm (SL2), respectively. The SLs do not change the magnetic properties of the Galfenol film, neither the anisotropy nor the boundary conditions for the magnon modes, but play the role of Bragg mirrors for the LA phonons [64,65]. Their non-overlapping stop bands are centred at 20 and 28.5 GHz, respectively, at the edge of the folded Brillouin zone. The SLs form two phononic cavities with different lengths between the corresponding SL and the open surface [66–68]. The FFT spectrum of the calculated coherent elastic response of the studied structure on the femtosecond optical excitation is shown in Fig. 3b. It includes a narrow spectral line at $f^1_{ph} = 20.0$ GHz and two spectrally close lines at $f^2_{ph} = 28.3$ GHz and $f^3_{ph} = 29.2$ GHz. The lowest spectral line corresponds to the phonon mode localized in the $Fe_{0.81}Ga_{0.19}$ layer. The higher-frequency pair corresponds to phonon modes localized between the open surface and the SL2. The idea of the experiment is to tune the frequency of the FM mode into resonance with the localized phonon mode by the external magnetic field. The field is applied in the film plane along the [100] crystallographic direction, and, like in the previous experiments (Section 3), the phonon-induced modulation of $\mathbf{B}_{\text{eff}}$ is given by the second-order magnetoelastic coefficient, b_4. Nevertheless, the magnon response to the ultrafast optical excitation drastically changes at the magnon-phonon resonance.

Fig. 3c – e illustrate the main experimental results. Fig. 3c shows the KR signal measured at $B = 100$ mT which corresponds to the magnon frequency being out of the phonon resonance in the film. The lifetime of the oscillation and the corresponding spectral width of the spectral line of 1.3 GHz in the FFT power spectrum agrees with the signal measured in the 120-nm film in a sample without SLs (here, the higher-order magnon modes are not resolved due to the shorter time window, in which $\psi(t)$ could be measured). The signal shown in Fig. 3d is significantly different at $B = 190$ mT at which $f_0 = f^1_{ph}$. The magnetization demonstrates long-living oscillations with the single frequency f_0. The field dependence of the spectral amplitude, A^1_{ph}, at $f = f^1_{ph}$ is shown in the inset in the right panel of Fig. 3d. The line at the frequency of the phonon mode is detectable in the whole range of external magnetic field, but achieves maximum amplitude at the resonant conditions, when the phonon driving dominates in the magnons response to the optical excitation.

The KR signal measured at $B = 400$ mT, when the magnon spectrum

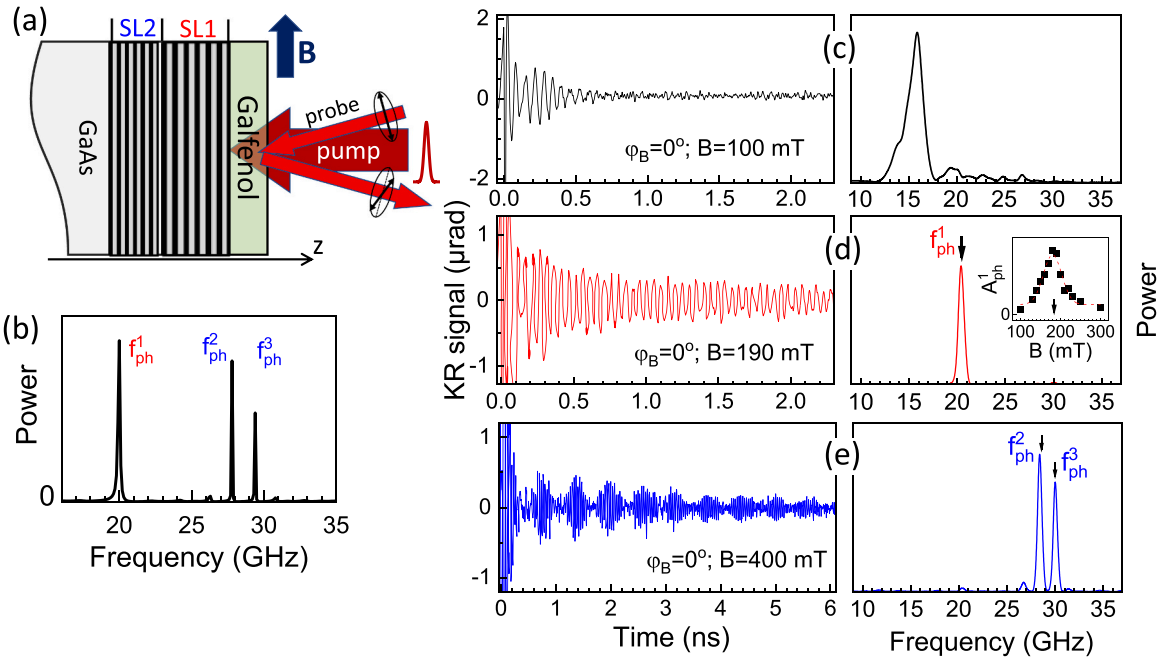

Fig. 3. Resonant phonon pumping of magnons in $Fe_{0.81}Ga_{0.19}$ phononic cavity [63]. (a) Scheme of the experiment, in which a 69-nm $Fe_{0.81}Ga_{0.19}$ film deposited on two superlattices (SL1 and SL2) plays the role of a phononic cavity hosting several phonon resonances. (b) Calculated spectrum of coherent phonons generated by the femtosecond pump laser pulse in the $Fe_{0.81}Ga_{0.19}$ film. (c) – (e) Kerr rotation signals (left panels) and their FFTs (right panels) for three strengths of the external magnetic field which tunes the fundamental magnon mode frequency: (c) out of resonance with the phonon modes; (d) in resonance with the first phonon mode; (e) in resonance with the second and third phonon modes. The inset in the right panel of (d) shows the magnetic field dependence of the spectral amplitude, A^1_{ph}, at the frequency of the first phonon mode in the transient KR signal.

overlaps with the second and third phonon modes is shown in Fig. 3e. The signal demonstrates a pronounced beating, and two spectral lines dominate in its FFT. Similar to the resonance with the SL1 phonon mode, the coherent magnon is purely "phononic" and the magnetization precession is determined by resonant phonon driving rather than by direct broadband optical excitation.

Phonon driving of the magnetization precession can be realized in various experimental geometries and using different structural designs, which support the formation of high-Q phonon modes: free standing films [69,70], lateral nanogratings [71,72], array of nanomagnets [16], and single nanomagnets embedded into a non-magnetic phononic resonator [73,74]. It has been realized in plain films excited by spatially modulated optical excitation (i.e., using the technique of transient gratings), which generates a standing surface acoustic wave [17,18]. The resonance phonon driving can be strong enough for observation of nonlinear effects, such as parametric frequency mixing of the magnon and phonon modes [75]. However, in most of ultrafast magnetoacoustic experiments the magnon-phonon interaction remains in the weak coupling regime and magnons and phonons remain unhybridized. Below we discuss the factors, which limit the formation of a hybridized magnon-phonon excitation, and present an approach which allows us to overcome these limitations.

5. Strong magnon-phonon coupling in Galfenol nanogratings

A direct manifestation of strong coupling of two excitations is the spectral splitting of the hybridized state at their resonance when the frequencies of the two interacting excitations coincide. It can be observed as avoided crossing of the dispersions at the intersection, when varying their detuning, or, in the transient signal, as beating pattern instead of independent, monochromatic oscillations at resonance condition, corresponding to the splitting of the FFT spectrum. The value of spectral splitting, Δ, is determined by the rate of the energy exchange, κ, between the two excitations: $\Delta = 2\kappa$. The splitting becomes observable, when the energy exchange occurs faster than the energy relaxation (or dephasing) for the interacting subsystems. This condition may be expressed through the cooperativity $C = \frac{4\kappa^2}{\gamma_1\gamma_2}$, where γ_1 and γ_2 are the characteristic decay rates of the separate excitations that are brought into resonance [39]. If $C > 1$, the coupling is strong and the hybridized state forms.

Strong magnon-phonon coupling was theoretically predicted for ferromagnetic metals [8,9], but was first confirmed, although indirectly, in low-frequency magnetoacoustic experiments with ferrimagnetic garnets [36,37]. These materials possess a relatively weak magnon-phonon interaction, but extremely low decay rates for both phonons and magnons provide a high coupling cooperativity. Moreover, in experiments with bulk waves in bulk materials, acoustic and spin waves with the same wavevectors perfectly match in space. Such favorable combination enables accumulation of the measurement signal over large propagation distances and/or long acquisition times, which makes indirect manifestations of strong coupling, e.g., altering the phonon polarization as predicted for the hybridized wave [76], well detectable.

In ultrafast magnetoacoustic experiments with metallic ferromagnetic nanostructures the magnon and phonon coherent responses to the ultrafast optical excitation enable the direct detection of the spectral splitting for the resonant conditions of the interacting phonon and magnon modes. However, both excitations in ferromagnetic metals possess much shorter lifetimes than in insulating garnets. The different boundary conditions for phonons and magnons and the mismatch of the magnetic and elastic anisotropies prevent the modes' spatial matching [77]. Moreover, the significant inequality in the energy flows between the optically excited coherent phonons and magnons, which results in phonon driving of the precession, can mask a small spectral splitting. The combination of these factors jeopardizes strong magnon-phonon coupling, whose observation in an ultrafast magnetoacoustic experiment until very recently [78–80] remained desirable but elusive.

We have demonstrated an approach to overcome these limitations in experiment [79] with Galfenol nanogratings illustrated in Fig. 4. The

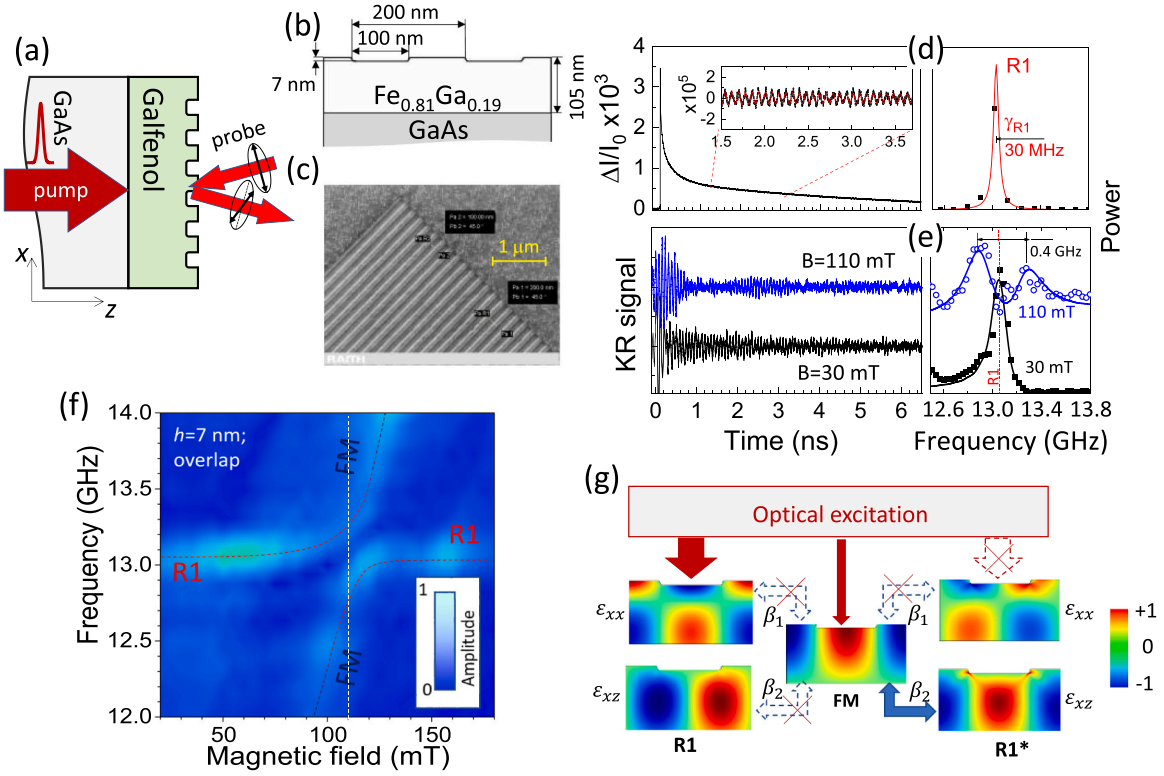

Fig. 4. Strong magnon-phonon coupling in a $Fe_{0.81}Ga_{0.19}$ nanograting [79]. (a) Scheme of the experiment with a $Fe_{0.81}Ga_{0.19}$ nanograting, which dimensions are shown in (b). (c) Scanning electron micrograph of the nanograting. (d) Transient reflectivity signal (left panel) and its FFT (right panel) obtained after subtraction of the slow decaying thermal background. The inset shows a zoomed section of the signal. (e) Transient KR signals measured at nonresonant ($B = 30$ mT) and resonant ($B = 110$ mT) magnetic fields (left panel) and their FFTs (right panel). The contribution of the Sezawa mode is filtered by a band block (14–16 GHz) Fourier filter. (f) Color map of the spectral density of the measured KR signal as a function of the external magnetic field. (g) Schematic illustration of the interaction of the R1 and R1 * phonon modes and the FM mode, determined by the spatial matching of the magnon mode with the uniaxial, ε_{xx}, and shear, ε_{xz}, strain components.

nanograting with the lateral size of $25 \times 25\ \mu m^2$ and the period $d = 200$ nm was formed by grooves of 100-nm width and 7-nm depth milled by a focused Ga-ion beam into a 105-nm $Fe_{0.81}Ga_{0.19}$film. In a pump-probe experiment carried out in the ASOPS scheme, the ferromagnetic layer is excited through the GaAs substrate by 1050-nm pump pulses focused to a spot of 5-μm diameter. The transient reflectivity and KR signals are measured using 780-nm probe pulses focused to a 1-μm-diameter spot at the front site, exactly opposite to the pump spot. An external magnetic field is applied in the sample plane at 45° to the groove's direction.

In the nanograting, in addition to the broad wavepacket of bulk longitudinal phonons, the pump laser pulse excites a number of surface phonon modes [81]. The strongest are the first- and second-order Rayleigh-like standing waves (the second-order mode is often referred to as Sezawa-wave). Both modes have the in-plane wave vector $q = \frac{2\pi}{d}$ set by the nanograting period and are characterized by three strain components: $\varepsilon_{xx}, \varepsilon_{zz}$, and ε_{xz}. Due to the mode symmetries, the first-order mode, which is further referred to as R1-mode, dominantly contributes to the transient reflectivity signal shown in Fig. 4d. The oscillations sitting on the slowly decaying thermal background has the frequency $f_{R1} = 13.1$ GHz in agreement with the calculated value of the R-mode eigenfrequency. The mode lifetime of 5.3 ns corresponds to the decay rate $\gamma_{R1} =$ 30 MHz and the Q-factor $Q_{R1} \approx 430$.

Because of the small depth of the grooves, which is much smaller than the Galfenol film thickness, the magnon spectrum of the nanograting is close to the spectrum of an un-patterned film [69,70] described in Section 3. It contains a set of discreet magnon modes quantized along the z-axis, which are additionally modulated along the x-axis [82,83]. The lowest quasi-uniform FM-mode remains dominating in the magnon spectrum and possesses the longest lifetime with the unaffected decay rate $\gamma_0 = 170$ MHz [69]. The interaction of magnons with both phonon modes of the nanograting was in the focus of the performed study. Here we present only the results related to the lowest R-mode, since they explicitly demonstrate a way to achieve strong magnon-phonon coupling.

Fig. 4e shows the transient KR signals, $\psi(t)$, and their FFT transforms in the spectral vicinity of the R-mode for two magnetic field strengths. At $B = 30$ mT, $f_0 \ll f_{R1}$ and the R1-mode contributes to the magnon kinetics through driving of higher-order magnon modes: the spectral line at the frequency of the R1-mode is well seen in the FFT spectra. At $B = 110$ mT, $f_0 = f_{R1}$, and the conditions of the magnon-phonon resonance are fulfilled. Here we detect a spectral line splitting around the R1-mode's spectral position with $\Delta = 400$ MHz, which exceeds both γ_{R1} and γ_0. The splitting of the magnon spectrum is also explicitly seen in the field dependence of the spectral density amplitude, shown as color map in Fig. 4f. There is a clear avoided crossing at the intersection of the field dependent FM-mode (highlighted by the white dashed line) and the R1-mode (highlighted by the red dashed line). This experimental manifestation directly indicates strong magnon-phonon coupling and hybridization of the FM- and R1-modes with the cooperativity $C \approx 32$ [84]. However here we do not observe an increase of the spectral amplitude at the frequency of the R1-mode for the condition of the magnon-phonon resonance.

To explain the formation of a hybridized state without energy transfer from coherent phonons to magnons (i.e. without phonon driving), we must consider the spatial matching of the interacting modes illustrated in Fig. 4g. Due to the spatial periodicity, the R1 mode has an antisymmetric counterpart, referred to as R1 * . The R1 and R1 * modes are spectrally degenerate. The symmetric R1 mode is excited by the laser pulse and contributes to the transient reflectivity signal, but the poor

match of all its strain components with the FM mode makes their interaction negligibly weak. The antisymmetric R1 * mode is "dark", i.e., not excited by the laser pulse. However, its shear (ε_{xz}) strain component perfectly matches the FM-mode. The interaction provided by the large first-order magnetoelastic coefficients (in contrast to the case of the plain film described in Section 4) results in the modes' strong coupling and hybridization.

A detailed numerical analysis of the modes' spatial matching and coupling strengths as well as a simplified model of the interacting harmonic oscillators, which explains the main experimental observations, may be found in Ref. [79].

6. Driving magnons by a propagating multimode phonon wavepacket

In Sections 4 and 5, we have considered the interaction of non-propagating phonon and magnon modes, examined for precise spatial overlap of the pump and probe pulses. Now we present the effect of magnon-phonon interaction for propagating excitations. Conventional experiments with electrically generated surface acoustic waves (SAWs) with frequencies up to several GHz have demonstrated two application-promising effects: strong and nonreciprocal attenuation of SAWs [85–88] and millimeter-distance driving of a "magnetization wave" by SAWs when the attenuation is minimized [89]. In the present section, we present the first experiments on driving of magnons by an optically generated propagating phonon wavepacket. Phonons with frequencies of about 10 GHz protected from scattering preserve their coherence and drive magnons at distances up to 100 μm, which corresponds to several hundreds of phonon wavelengths.

The studied structure and experimental scheme are shown in Fig. 5a. The Galfenol film of 105-nm thickness is grown on a 10-period GaAs (59 nm)/AlAs (72 nm) superlattice deposited on the GaAs substrate. The film surface is patterned by FIB-milling to a nanograting with the period $d = 200$ nm. The grooves' width and depth are 100 and 25 nm, respectively. In this experiment, the superlattice plays the role of a phononic waveguide. It has a higher acoustic impedance than both the GaAs substrate and Galfenol film and hosts Lamb-like phonon modes localized between the substrate and the Galfenol film [90]. In the experiment, coherent phonons are excited by the pump pulse focused to a spot of the diameter $\sigma = 1$ μm (at the $1/\sqrt{e}$ level of the Gaussian intensity distribution) on the backside of the Galfenol film. The spectrum of generated coherent phonons shown in Fig. 5b includes two types of phonon modes which propagate parallel to the surface: Rayleigh-like modes (R1 and R2 discussed in Section 5); and a wavepacket of 22 Lamb-like phonon modes (W-modes) localized in the SL, which frequencies are in the range between 16 and 18 GHz. The Gaussian distribution of the wavevectors in these modes is centred at $q = \frac{2\pi}{d}$ and has a width of $1/\sigma$ (also at the $1/\sqrt{e}$ level). The R1-, R2-, and W- phonon wavepackets consisting of coherent phonons with specific polarizations propagate along the reciprocal wavevector of the nanograting with velocities set by the modes' dispersions. The R1 and R2 modes decay on distances of about 10 μm due to scattering on the patterned surface [91]. The wavepacket of W modes guided by the SL underneath the surface propagates on significantly larger distances. The mode dispersions, spatial profiles, and details of their excitation and detection may be found in Ref. [90].

In a nanograting of large depth, the magnon spectrum is enriched and broadened by magnetostatic modes modulated along the x-axis due to the strong periodic modulation of the demagnetizing field [82,83]. The spectrally close magnetostatic and exchange modes form a quasi-continuous magnon spectrum with the lowest frequency corresponding to the quasi-uniform FM mode. As a result, the interaction between the propagating multimode phonon wavepacket and the magnon modes of the nanograting is non-selective, neither spectrally nor spatially, and the propagating coherent phonons drive the broadband "magnetization wave" along the surface.

Several KR signals and their FFTs measured at varied distances, L, between the pump and probe spots are shown in Fig. 5c. The signals are measured at $B = 100$ mT, at which $f_0 = 10$ GHz, and all the phonon modes fall into the magnon spectrum of the nanograting. At small propagation distances, $\psi(t)$ consists of the leading W mode wavepacket and the following tail of the surface modes, which propagate with lower velocity. The FFTs of the signals measured at $L = 6$ and 10 μm contain the spectral lines at their corresponding spectral positions. The red and blue curves in the inset of the signal spectrum panel measured at $L = 10$ μm are the FFTs calculated for the two separate time windows shown by the dashed frames of the same colour in the signal panel. The comparison of spectral amplitudes of the R and W modes emphasizes their time distribution in the magnon response. The phonon-driven "magnetization wave" remains detectable for distances up to 80 μm (limited by the nanograting length), but starting from 20-μm distance it is driven solely by the W mode wavepacket. Despite the broad spectra of both

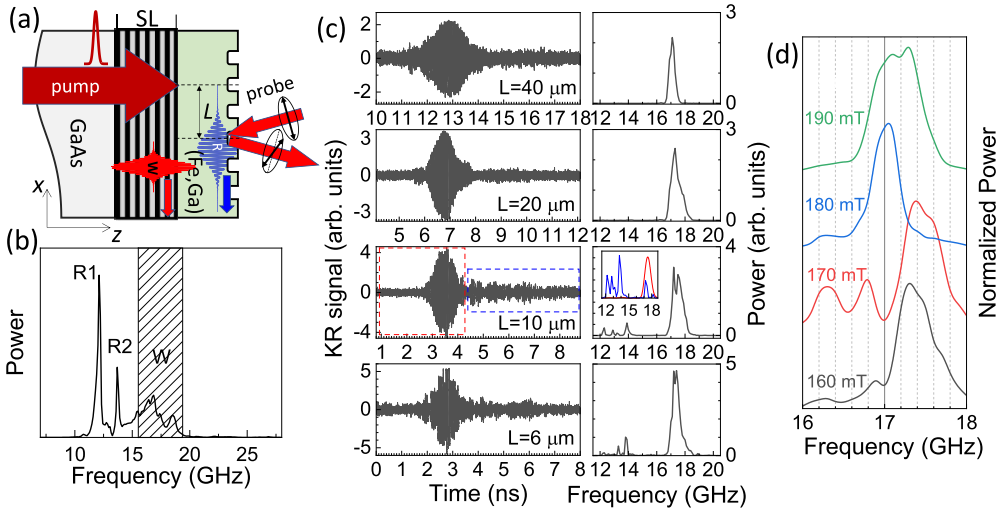

Fig. 5. Driving magnons by a guided multimode phonon wavepacket. (a) Scheme of the experiment with a $Fe_{0.81}Ga_{0.19}$ nanograting deposited on a multimode phonon waveguide formed by a GaAs/AlAs superlattice. (b) FFT spectrum of the transient reflectivity signal. The dashed rectangle shows the spectral band of the guided phonon modes (W-modes). (c) Transient KR signals (left panels) and their FFTs (right panels) measured at the varied distance, L, between the pump and probe laser spots for $B = 100$ mT. (d) Normalized FFTs of the transient KR signals measured at $L = 20$ μm for different external magnetic fields.

excitations, the spatial-temporal profile and spectral content of $\psi(t)$ measured at $L = 20$ μm demonstrate a strong dependence on the external magnetic filed. The variation of $\psi(t)$ with B increasing from 160 to 190 mT is clearly seen in Fig. 5d. This volatility is due to the superposition of many spectrally close phonon and magnon modes at the detection point. The change of magnetic field changes the spectral overlap of the interacting modes and thus the spectral content of the signal. This behaviour drastically differs from the case of a monochromatic surface acoustic wave, when only the amplitude of phase of the magnon transient depends on L and B [89].

7. Conclusions

We have reviewed a number of ultrafast magnetoacoustic experiments with Galfenol-based nanostructures, in which magnon-phonon interaction plays a crucial role in the coherent magnon response to the ultrafast optical excitation. The demonstrated effects are of fundamental nature, but their strong manifestation is largely determined by the unique properties of Galfenol. The pronounced magnetocrystalline anisotropy makes possible to turn on and off the contribution of the magnon-phonon interaction to the magnon kinetics. In the exploited high-symmetry films, this opportunity is minimally utilized. However, in Galfenol films grown on low-symmetry substrates, in which the magnetocrystalline and shape anisotropy are not coplanar, the possibilities of controlling the contribution of coherent phonons are much wider [52]. The small decay rates significantly increase the efficiency of the resonant magnon-phonon interaction up to the formation of a hybridized state in the strong coupling regime. The technological friendliness of Galfenol enables one to control the spectrum of phonon and magnon modes through the structural design and, consequently, vary the magnon response to optical excitation. We have shown how multimode precession characterized by fast dephasing can be transformed into monochromatic oscillations of long lifetime by resonant phonon driving. On the contrary, the mode composition of a coherent magnon wavepacket can be significantly broadened by the interaction with a multimode phonon wavepacket. The resulting collective excitation, delivered to a distance unattainable for pure spin waves [92], exhibits ultimate spectral variability.

The demonstrated effects have broad application perspectives. The narrow band phonon driving of the magnetization precession enables generation of pure spin currents (without transfer of charge) [93]. This approach, if realized in nanolayers with high-frequency phonon resonances, will extend the available frequencies up to the Terahertz range. The same approach realized in nonplanar structures makes possible the generation of microwave magnetic fields of high amplitudes (thanks to the Galfenol large saturation magnetization) and nanoscale localization [71]. This solution is a powerful alternative to spin-torque nano--oscillators driven by high-density electric currents. In the applications considered above, laser sources with a high pulse repetition rate have excellent prospects. Resonant excitation of coherent magnons with phase and wavevector locking has been demonstrated using solid-state lasers with repetition rates of 1 and 10 GHz [94,95]. In turn, excitation of coherent phonons has been realized by means of a miniature semiconductor mode-locked laser with a repetition rate of 16 GHz [96]. Combining these approaches paves the way for constructing miniature phonon-driven generators of spin currents and ac- magnetic fields for applications outside a the research lab containing bulky equipment such as optical tables etc.

Our results have potential for quantum operations and neuromorphic computing. The hybridized magnon-phonon excitation, which possesses tunability of magnons and robustness of phonons, may enable fine operations at the quantum level [47,48]. Here it is especially attractive to realize the transport of hybridized excitations between spatially separated “write in” and “read out” ports. The variability and extreme volatility of multimode magnon-phonon wavepackets suggests using them as information carriers in neural networks [97]. These directions require and stimulate further concerted research efforts.

Declaration of Competing Interest

The authors declare that they have no known competing financial interests or personal relationships that could have appeared to influence the work reported in this paper.

Data availability

Data will be made available on request.

Acknowledgements

The studies presented in this review were supported by the Bundesministerium fur Bildung und Forschung through the project VIP+ “Nanomagnetron”, by the Deutsche Forschungsgemeinschaft by the project SFB TRR 160 (Projects B6 and A1) and the Engineering and Physical Sciences Research Council (Grant No. EP/V056557/1). The cooperation between TU Dortmund and the Lashkaryov Institute was supported by the Volkswagen Foundation (grant no. 97758). T.L.L. acknowledges the Alexander von Humboldt Foundation support through the Philipp Schwartz Initiative and TU Dortmund core funds.

We dedicate this manuscript to the memory of Boris Glavin (*Department of Theoretical Physics, V.E. Lashkaryov Institute of Semiconductor Physics in Kyiv)*, who passed away in the summer of 2018 in a tragic accident. His calculations and imagination based on a deep understanding of physics were a main driving force right from the start of the ultrafast acoustics activities of the Dortmund and Nottingham teams. We still miss him and his pleasant character evidenced in numerous discussions not only about physics sorely.

References

[1] O. Matsuda, M.C. Larciprete, R. Li Voti, O.B. Wright, Fundamentals of picosecond laser ultrasonics, Ultrasonics 56 (2015) 3–20, https://doi.org/10.1016/j.ultras.2014.06.005.

[2] A. Kirilyuk, A.V. Kimel, T. Rasing, Ultrafast optical manipulation of magnetic order, Rev. Mod. Phys. 82 (3) (2010) 2731–2784, https://doi.org/10.1103/RevModPhys.82.2731.

[3] A.M. Kalashnikova, A.V. Kimel, R.V. Pisarev, Phys. -Usp. 58 (10) (2015) 968–980, https://doi.org/10.3367/UFNe.0185.201510j.1064.

[4] A. Thomsen, J. Strait, Z. Vardeny, H. Maris, J. Tauc, J. Hauser, Coherent phonon generation and detection by picosecond light pulses, Phys. Rev. Lett. 53 (10) (1984) 989–992, https://doi.org/10.1103/PhysRevLett.53.989.

[5] A. Thomsen, H.T. Grahn, H.J. Maris, J. Tauc, Surface generation and detection of phonons by picosecond light pulses, Phys. Rev. B Condens. Matter 34 (6) (1986) 4129–4138, https://doi.org/10.1103/PhysRevB.34.4129.

[6] G.L. Eesley, B.M. Clemens, C.A. Paddock, Generation and detection of picosecond acoustic pulses in thin metal films, Appl. Phys. Lett. 50 (12) (1987) 717–719, https://doi.org/10.1063/1.98077.

[7] E. Beaurepaire, J.C. Merle, A. Daunois, J.Y. Bigot, Ultrafast spin dynamics in ferromagnetic nickel, Phys. Rev. Lett. 76 (22) (1996) 4250–4253, https://doi.org/10.1103/PhysRevLett.76.4250.

[8] M. van Kampen, C. Jozsa, J.T. Kohlhepp, P. LeClair, L. Lagae, W.J.M. de Jonge, B. Koopmans, All-optical probe of coherent spin waves, Phys. Rev. Lett. 88 (22) (2002), 227201, https://doi.org/10.1103/PhysRevLett.88.227201.

[9] C. Kittel, Interaction of spin waves and ultrasonic waves in ferromagnetic crystals, Phys. Rev. 110 (4) (1958) 836–841, https://doi.org/10.1103/PhysRev.110.836.

[10] A.I. Akhiezer, V.G. Bar'iakhtar, S.V. Peletminskii, Coupled magnetoelastic waves in ferromagnetic media and ferroacoustic resonance, Sov. Phys. JETP 35 (8) (1959) 157–164.

[11] A.V. Scherbakov, A.S. Salasyuk, A.V. Akimov, X. Liu, M. Bombeck, C. Bruggemann, D.R. Yakovlev, V.F. Sapega, J.K. Furdyna, M. Bayer, Coherent magnetization precession in ferromagnetic (Ga,Mn)As induced by picosecond acoustic pulses, Phys. Rev. Lett. 105 (2010), 117204, https://doi.org/10.1103/PhysRevLett.105.117204.

[12] M. Bombeck, A.S. Salasyuk, B.A. Glavin, A.V. Scherbakov, C. Bruggemann, D. R. Yakovlev, V.F. Sapega, X. Liu, J.K. Furdyna, A.V. Akimov, M. Bayer, Excitation of spin waves in ferromagnetic (Ga,Mn)As layers by picosecond strain pulses, Phys. Rev. B 85 (2012), 195324, https://doi.org/10.1103/PhysRevB.85.195324.

[13] J.-W. Kim, M. Vomir, J.-Y. Bigot, Ultrafast magnetoacoustics in nickel films, Phys. Rev. Lett. 109 (2012), 166601, https://doi.org/10.1103/PhysRevLett.109.166601.

[14] J.V. Jäger, A.V. Scherbakov, T.L. Linnik, D.R. Yakovlev, M. Wang, P. Wadley, V. Holy, S.A. Cavill, A.V. Akimov, A.W. Rushforth, M. Bayer, Picosecond inverse

magnetostriction in Galfenol thin films, Appl. Phys. Lett. 103 (2013), 032409, https://doi.org/10.1063/1.4816014.
[15] D. Afanasiev, I. Razdolski, K.M. Skibinsky, D. Bolotin, S.V. Yagupov, M. B. Strugatsky, A. Kirilyuk, Th Rasing, A.V. Kimel, Laser excitation of lattice-driven anharmonic magnetization dynamics in dielectric $FeBO_3$, Phys. Rev. Lett. 112 (2014), 147403, https://doi.org/10.1103/PhysRevLett.112.147403.
[16] Y. Yahagi, B. Harteneck, S. Cabrini, H. Schmidt, Controlling nanomagnet magnetization dynamics via magnetoelastic coupling, 140405(R), Phys. Rev. B 90 (2014), https://doi.org/10.1103/PhysRevB.90.140405.
[17] J. Janušonis, C.L. Chang, P.H.M. van Loosdrecht, R.I. Tobey, Frequency tunable surface magneto elastic waves, Appl. Phys. Lett. 106 (2015), 181601, https://doi.org/10.1063/1.4919882.
[18] J. Janušonis, C.L. Chang, T. Jansma, A. Gatilova, V.S. Vlasov, A.M. Lomonosov, V. V. Temnov, R.I. Tobey, Ultrafast magnetoelastic probing of surface acoustic transients, Phys. Rev. B 94 (2016), 024415, https://doi.org/10.1103/PhysRevB.94.024415.
[19] M. Deb, E. Popova, M. Hehn, N. Keller, S. Mangin, G. Malinowski, Picosecond acoustic-excitation-driven ultrafast magnetization dynamics in dielectric Bi-substituted yttrium iron garnet, Phys. Rev. B 98 (2018), 174407, https://doi.org/10.1103/PhysRevB.98.174407.
[20] Y. Hashimoto, D. Bossini, T.H. Johansen, E. Saitoh, A. Kirilyuk, T. Rasinget, Frequency and wavenumber selective excitation of spin waves through coherent energy transfer from elastic waves, 140404(R), Phys. Rev. B 97 (2018), https://doi.org/10.1103/PhysRevB.97.140404.
[21] M. Deb, E. Popova, M. Hehn, N. Keller, S. Petit-Watelot, M. Bargheer, S. Mangin, G. Malinowski, Femtosecond laser-excitation-driven high frequency standing spin waves in nanoscale dielectric thin films of Iron Garnets, Phys. Rev. Lett. 123 (2019), 027202, https://doi.org/10.1103/PhysRevLett.123.027202.
[22] D.-L. Zhang, J. Zhu, T. Qu, D.M. Lattery, R.H. Victora, X. Wang, J.-P. Wang, High-frequency magnetoacoustic resonance through strain-spin coupling in perpendicular magnetic multilayers, Sci. Adv. 6 (2020) eabb4607, https://doi.org/10.1126/sciadv.abb4607.
[23] T. Parpiiev, A. Hillion, V. Vlasov, V. Gusev, K. Dumesnil, T. Hauet, S. Andrieu, A. Anane, T. Pezeril, Ultrafast strain excitation in highly magnetostrictive terfenol: Experiments and theory, Phys. Rev. B 104 (2021), 224426, https://doi.org/10.1103/PhysRevB.104.224426.
[24] S.P. Zeuschner, X.-G. Wang, M. Deb, E. Popova, G. Malinowski, M. Hehn, N. Keller, J. Berakdar, M. Bargheer, Standing spin wave excitation in Bi: YIG films via temperature-induced anisotropy changes and magneto-elastic coupling, Phys. Rev. B 106 (2022), 134401, https://doi.org/10.1103/PhysRevB.106.134401.
[25] A. Alekhin, A.M. Lomonosov, N. Leo, M. Ludwig, V.S. Vlasov, L. Kotov, A. Leitenstorfer, P. Gaal, P. Vavassori, V. Temnov, Quantitative ultrafast magnetoacoustics at magnetic metasurfaces, Nano Lett. (2023), https://doi.org/10.1021/acs.nanolett.3c02336.
[26] T.L. Linnik, A.V. Scherbakov, D.R. Yakovlev, X. Liu, J.K. Furdyna, M. Bayer, Theory of magnetization precession induced by a picosecond strain pulse in ferromagnetic semiconductor (Ga,Mn)As, Phys. Rev. B 84 (2011), 214432, https://doi.org/10.1103/PhysRevB.84.214432.
[27] O. Kovalenko, T. Pezeril, V.V. Temnov, New concept for magnetization switching by ultrafast acoustic pulses, Phys. Rev. Lett. 110 (2013), 266602, https://doi.org/10.1103/PhysRevLett.110.266602.
[28] K. Shen, G.E.W. Bauer, Laser-induced spatiotemporal dynamics of magnetic films, Phys. Rev. Lett. 115 (2015), 197201, https://doi.org/10.1103/PhysRevLett.115.197201.
[29] A.V. Azovtsev, N.A. Pertsev, Magnetization dynamics and spin pumping induced by standing elastic waves, Phys. Rev. B 94 (2016), 184401, https://doi.org/10.1103/PhysRevB.94.184401.
[30] K. Shen, G.E.W. Bauer, Theory of spin and lattice wave dynamics excited by focused laser pulses, J. Phys. D: Appl. Phys. 51 (22) (2018), 224008, https://doi.org/10.1088/1361-6463/aabd68.
[31] A.V. Azovtsev, N.A. Pertsev, Excitation of high-frequency magnon modes in magnetoelastic films by short strain pulses, Phys. Rev. Mater. 4 (2020), 064418, https://doi.org/10.1103/PhysRevMaterials.4.064418.
[32] V.S. Vlasov, A.M. Lomonosov, A.V. Golov, L.N. Kotov, V. Besse, A. Alekhin, D. A. Kuzmin, I.V. Bychkov, V.V. Temnov, Magnetization switching in bistable nanomagnets by picosecond pulses of surface acoustic waves, Phys. Rev. B 101 (2020), 024425, https://doi.org/10.1103/PhysRevB.101.024425.
[33] V. Besse, A.V. Golov, V.S. Vlasov, A. Alekhin, D. Kuzmin, I.V. Bychkov, L.N. Kotov, V.V. Temnov, Generation of exchange magnons in thin ferromagnetic films by ultrashort acoustic pulses, J. Magn. Magn. Mater. 502 (2020), 166320, https://doi.org/10.1016/j.jmmm.2019.166320.
[34] A.V. Azovtsev, N.A. Pertsev, Acoustically excited magnetic dynamics and spin flow in spin-valve structures, Phys. Rev. Appl. 17 (2022), 034070, https://doi.org/10.1103/PhysRevApplied.17.034070.
[35] U. Vernik, A.M. Lomonosov, V.S. Vlasov, L.N. Kotov, D.A. Kuzmin, I.V. Bychkov, P. Vavassori, V.V. Temnov, Resonant phonon-magnon interactions in free-standing metal-ferromagnet multilayer structures, Phys. Rev. B 106 (2022), 144420, https://doi.org/10.1103/PhysRevB.106.144420.
[36] J.W. Tucker, V. Rampton, Microwave Ultrasonics in Solid State Physics, North-Holland, 1972, pp. 134–183.
[37] O. Yu. Belyaeva, S.N. Karpachev, L.K. Zarembo, Magnetoacoustics of ferrites and magnetoacoustic resonance, Sov. Phys. Usp. 35 (2) (1992) 106–122, https://doi.org/10.1070/PU1992v035n02ABEH002216.
[38] I. Tudosa, C. Stamm, A.B. Kashuba, F. King, H.C. Siegmann, J. Stöhr, G. Ju, B. Lu, D. Weller, The ultimate speed of magnetic switching in granular recording media, Nature 428 (2004) 831–833, https://doi.org/10.1038/nature02438.
[39] L. Thevenard, J.-Y. Duquesne, E. Peronne, H.J. von Bardeleben, H. Jaffres, S. Ruttala, J.-M. George, A. Lemaître, C. Gourdon, Irreversible magnetization switching using surface acoustic waves, Phys. Rev. B 87 (2013), 144402, https://doi.org/10.1103/PhysRevB.87.144402.
[40] A. Stupakiewicz, C.S. Davies, K. Szerenos, D. Afanasiev, K.S. Rabinovich, A. V. Boris, A. Caviglia, A.V. Kimel, A. Kirilyuk, Ultrafast phononic switching of magnetization, Nat. Phys. 17 (2021) 489–492, https://doi.org/10.1038/s41567-020-01124-9.
[41] D.E. Nikonov, I.A. Young, Benchmarking of beyond-CMOS exploratory devices for logic integrated circuits, IEEE J. Explor. Solid-State Comput. 1 (2015) 3–11, https://doi.org/10.1109/JXCDC.2015.2418033.
[42] Y. Katayama, T. Yamane, D. Nakano, R. Nakane, G. Tanaka, Wave-based neuromorphic computing framework for brain-like energy efficiency and Integration, IEEE Trans. Nanotechnol. 15 (5) (2016) 762–769, https://doi.org/10.1109/TNANO.2016.2545690.
[43] P. Delsing, et al., The 2019 surface acoustic waves roadmap, J. Phys. D: Appl. Phys. 52 (35) (2019), 353001, https://doi.org/10.1088/1361-6463/ab1b04.
[44] A.A. Clerk, K.W. Lehnert, P. Bertet, J.R. Petta, Y. Nakamura, Hybrid quantum systems with circuit quantum electrodynamics, Nat. Phys. 16 (2020) 257–267, https://doi.org/10.1038/s41567-020-0797-9.
[45] A. Barman, et al., The 2021 magnonics roadmap, J. Phys.: Condens. Matter 33 (41) (2021), 413001, https://doi.org/10.1088/1361-648X/abec1a.
[46] Y. Li, C. Zhao, W. Zhang, A. Hoffmann, V. Novosad, Advances in coherent coupling between magnons and acoustic phonons, APL Mater. 9 (2021), 060902, https://doi.org/10.1063/5.0047054.
[47] D. Awschalom, et al., Quantum engineering with hybrid magnonics systems and materials, IEEE Trans. Quantum Eng. 2 (2021), 5500836, https://doi.org/10.1109/TQE.2021.3057799.
[48] H.Y. Yuan, et al., Quantum magnonics: when magnon spintronics meet the quantum information science, Phys. Rep. 965 (2022) 1–74, https://doi.org/10.1016/j.physrep.2022.03.002.
[49] J. Atulasimha, A.B.A. Flatau, A review of magnetostrictive iron-gallium alloys, Smart Mater. Struct. 20 (4) (2011), 043001, https://doi.org/10.1088/0964-1726/20/4/043001.
[50] D.E. Parkes, S.A. Cavill, A.T. Hindmarch, P. Wadley, F. McGee, C.R. Staddon, K. W. Edmonds, R.P. Campion, B.L. Gallagher, A.W. Rushforth, Non-volatile voltage control of magnetization and magnetic domain walls in magnetostrictive epitaxial thin films, Appl. Phys. Lett. 101 (2012), 072402, https://doi.org/10.1063/1.4745789.
[51] D.E. Parkes, L.R. Shelford, P. Wadley, V. Holý, M. Wang, A.T. Hindmarch, G. van der Laan, R.P. Campion, K.W. Edmonds, S.A. Cavill, A.W. Rushforth, Magnetostrictive thin films for microwave spintronics, Sci. Rep. 3 (2013) 2220, https://doi.org/10.1038/srep02220.
[52] V.N. Kats, T.L. Linnik, A.S. Salasyuk, A.W. Rushforth, M. Wang, P. Wadley, A. V. Akimov, S.A. Cavill, V. Holy, A.M. Kalashnikova, A.V. Scherbakov, Ultrafast changes of magnetic anisotropy driven by laser-generated coherent and non-coherent phonons in metallic films, Phys. Rev. B 93 (2016), 214422, https://doi.org/10.1103/PhysRevB.93.214422.
[53] A.G. Gurevich, G.A. Melkov. Magnetization Oscillations and Waves, 1st edition.,, Taylor & Francis, London, 1996, 464 p.
[54] W.K. Hiebert, A. Stankiewicz, M.R. Freeman, Direct observation of magnetic relaxation in a small permalloy disk by time-resolved scanning kerr microscopy, Phys. Rev. Lett. 79 (6) (1997) 1134–1137, https://doi.org/10.1103/PhysRevLett.79.1134.
[55] A. Bartelsa, R. Cerna, C. Kistner, A. Thoma, F. Hudert, C. Janke, T. Dekorsy, Ultrafast time-domain spectroscopy based on high speed asynchronous optical sampling, Rev. Sci. Instrum. 78 (2007), 035107, https://doi.org/10.1063/1.2714048.
[56] A.E. Clark, K.B. Hathaway, M. Wun-Fogle, J.B. Restorff, T.A. Lograsso, V. M. Keppens, G. Petculescu, R.A. Taylor, Extraordinary magnetoelasticity and lattice softening in bcc Fe-Ga alloys, J. Appl. Phys. 93 (2003) 8621–8623, https://doi.org/10.1063/1.1540130.
[57] A.E. Clark, M. Wun-Fogle, J.B. Restorff, K.W. Dennis, T.A. Lograsso, R. W. McCallum, Temperature dependence of the magnetic anisotropy and magnetostriction of $Fe_{100-x}Ga_x$ ($x = 8.6, 16.6, 28.5$), J. Appl. Phys. 97 (2005) 10M316, https://doi.org/10.1063/1.1856731.
[58] J.B. Restorff, M. Wun-Fogle, K.B. Hathaway, A.E. Clark, T.A. Lograsso, G. Petculescu, Tetragonal magnetostriction and magnetoelastic coupling in Fe-Al, Fe-Ga, Fe-Ge, Fe-Si,Fe-Ga-Al, and Fe-Ga-Ge alloys, J. Appl. Phys. 111 (2012), 023905, https://doi.org/10.1063/1.3674318.
[59] A.V. Scherbakov, A.P. Danilov, F. Godejohann, T.L. Linnik, B.A. Glavin, L. A. Shelukhin, D.P. Pattnaik, M. Wang, A.W. Rushforth, D.R. Yakovlev, A. V. Akimov, M. Bayer, Optical excitation of single- and multimode magnetization precession in Fe-Ga nanolayers, 031003(R), Phys. Rev. Appl. 11 (2019), https://doi.org/10.1103/PhysRevApplied.11.031003.
[60] Y. Fan, H.B. Zhao, G. Lupke, A.T. Hanbicki, C.H. Li, B.T. Jonker, Anisotropic exchange coupling and stress-induced uniaxial magnetic anisotropy in Fe/GaAs (001), Phys. Rev. B 85 (2012), 165311, https://doi.org/10.1103/PhysRevB.85.165311.
[61] D.B. Gopman, V. Sampath, H. Ahmad, S. Bandyopadhyay, J. Atulasimha, Static and dynamic magnetic properties of sputtered Fe-Ga thin films, IEEE Trans. Magn. 53 (11) (2017), 6101304, https://doi.org/10.1109/TMAG.2017.2700404.
[62] C. Kittel, Excitation of spin waves in a ferromagnet by a uniform rf field, Phys. Rev. 110 (1958) 1295–1297, https://doi.org/10.1103/PhysRev.110.1295.
[63] J.V. Jäger, A.V. Scherbakov, B.A. Glavin, A.S. Salasyuk, R.P. Campion, A. W. Rushforth, D.R. Yakovlev, A.V. Akimov, M. Bayer, Resonant driving of

magnetization precession in a ferromagnetic layer by coherent monochromatic phonons, 020404(R), Phys. Rev. B 92 (2015), https://doi.org/10.1103/PhysRevB.92.020404.
[64] M. Trigo, T.A. Eckhause, M. Reason, R.S. Goldman, R. Merlin, Observation of surface-avoiding waves: a new class of extended states in periodic media, Phys. Rev. Lett. 97 (2006), 124301, https://doi.org/10.1103/PhysRevLett.97.124301.
[65] N.D. Lanzillotti-Kimura, B. Perrin, A. Fainstein, B. Jusserand, A. Lemaître, Nanophononic thin-film filters and mirrors studied by picosecond ultrasonics, Appl. Phys. Lett. 96 (2010), 053101, https://doi.org/10.1063/1.3295701.
[66] M.F. Pascual Winter, G. Rozas, A. Fainstein, B. Jusserand, B. Perrin, A. Huynh, P. O. Vaccaro, S. Saravanan, Selective optical generation of coherent acoustic nanocavity modes, Phys. Rev. Lett. 98 (2007), 265501, https://doi.org/10.1103/PhysRevLett.98.265501.
[67] N.D. Lanzillotti-Kimura, A. Fainstein, B. Perrin, B. Jusserand, A. Soukiassian, X. X. Xi, D.G. Schlom, Enhancement and inhibition of coherent phonon emission of a Ni film in a $BaTiO_3/SrTiO_3$ cavity, Phys. Rev. Lett. 104 (2010), 187402, https://doi.org/10.1103/PhysRevLett.104.187402.
[68] N.D. Lanzillotti-Kimura, A. Fainstein, B. Jusserand, Towards GHz–THz cavity optomechanics in DBR-based semiconductor resonators, Ultrasonics 56 (2015) 80–89, https://doi.org/10.1016/j.ultras.2014.05.017.
[69] J.-W. Kim, J.-Y. Bigot, Magnetization precession induced by picosecond acoustic pulses in a freestanding film acting as an acoustic cavity, Phys. Rev. B 95 (2017), 144422, https://doi.org/10.1103/PhysRevB.95.144422.
[70] A. Ghita, T.-G. Mocioi, A.M. Lomonosov, J. Kim, O. Kovalenko, P. Vavassori, V. V. Temnov, Anatomy of ultrafast quantitative magnetoacoustics in freestanding nickel thin films, Phys. Rev. B 107 (2023), 134419, https://doi.org/10.1103/PhysRevB.107.134419.
[71] A.S. Salasyuk, A.V. Rudkovskaya, A.P. Danilov, B.A. Glavin, S.M. Kukhtaruk, M. Wang, A.W. Rushforth, P.A. Nekludova, S.V. Sokolov, A.A. Elistratov, D. R. Yakovlev, M. Bayer, A.V. Akimov, A.V. Scherbakov, Generation of a localized microwave magnetic field by coherent phonons in a ferromagnetic nanograting, 060404(R), Phys. Rev. B 97 (2018), https://doi.org/10.1103/PhysRevB.97.060404.
[72] C.L. Chang, R.R. Tamming, T.J. Broomhall, J. Janusonis, P.W. Fry, R.I. Tobey, T. J. Hayward, Selective excitation of localized spin-wave modes by optically pumped surface acoustic waves, Phys. Rev. Appl. 10 (2018), 034068, https://doi.org/10.1103/PhysRevApplied.10.034068.
[73] W.G. Yang, M. Jaris, C. Berk, H. Schmidt, Preferential excitation of a single nanomagnet using magnetoelastic coupling, Phys. Rev. B 99 (2019), 104434, https://doi.org/10.1103/PhysRevB.99.104434.
[74] W.G. Yang, H. Schmidt, Acoustic control of magnetism toward energy-efficient applications, Phys. Rev. Appl. 8 (2021), 021304, https://doi.org/10.1063/5.0042138.
[75] C.L. Chang, A.M. Lomonosov, J. Janusonis, V.S. Vlasov, V.V. Temnov, R.I. Tobey, Parametric frequency mixing in a magnetoelastically driven linear ferromagnetic-resonance oscillator, 060409(R), Phys. Rev. B 95 (2017), https://doi.org/10.1103/PhysRevB.95.060409.
[76] H. Matthews, R. Le Craw, Acoustic wave rotation by magnon-phonon Interaction, Phys. Rev. Lett. 8 (10) (1962) 397–400, https://doi.org/10.1103/PhysRevLett.8.397.
[77] N.K.P. Babu, A. Trzaskowska, P. Graczyk, G. Centała, S. Mieszczak, H. Głowiński, M. Zdunek, S. Mielcarek, J.W. Kłos, The interaction between surface acoustic waves and spin waves: the role of anisotropy and spatial profiles of the modes, Nano Lett. 21 (2) (2021) 946–951, https://doi.org/10.1021/acs.nanolett.0c03692.
[78] C. Berk, M. Jaris, W. Yang, S. Dhuey, S. Cabrini, H. Schmidt, Strongly coupled magnon-phonon dynamics in a single nanomagnet, Nat. Commun. 10 (2019) 2652, https://doi.org/10.1038/s41467-019-10545-x.
[79] F. Godejohann, A.V. Scherbakov, S.M. Kukhtaruk, A.N. Poddubny, D. D. Yaremkevich, M. Wang, A. Nadzeyka, D.R. Yakovlev, A.W. Rushforth, A. V. Akimov, M. Bayer, Magnon polaron formed by selectively coupled coherent magnon and phonon modes of a surface patterned ferromagnet, Phys. Rev. B 102 (2020), 144438, https://doi.org/10.1103/PhysRevB.102.144438.
[80] T. Hioki, Y. Hashimoto, E. Saitoh, Coherent oscillation between phonons and magnons, Commun. Phys. 5 (2022) 115, https://doi.org/10.1038/s42005-022-00888-1.
[81] D. Nardi, M. Travagliati, M.E. Siemens, Q. Li, M.M. Murnane, H.C. Kapteyn, G. Ferrini, F. Parmigiani, F. Banfi, Probing thermomechanics at the nanoscale: Impulsively excited pseudosurface acoustic waves in hypersonic phononic crystals, Nano Lett. 11 (10) (2011) 4126–4133, https://doi.org/10.1021/nl201863n.
[82] M. Langer, R.A. Gallardo, T. Schneider, S. Stienen, A. RoldánMolina, Y. Yuan, K. Lenz, J. Lindner, P. Landeros, J. Fassbender, Spin-wave modes in transition from a thin film to a full magnonic crystal, Phys. Rev. B 99 (2019), 024426, https://doi.org/10.1103/PhysRevB.99.024426.
[83] S.M. Kukhtaruk, A.W. Rushforth, F. Godejohann, A.V. Scherbakov, M. Bayer, Transition magnon modes in thin ferromagnetic nanogratings, Phys. Rev. B 106 (2021), 064411, https://doi.org/10.1103/PhysRevB.106.064411.
[84] In the original paper [67], we calculated the cooperativity as $C = \kappa^2/\gamma_{R1}\gamma_{FM} \approx 8$, which is four times smaller than the value $C \approx 32$calculated in this review in accordance with the commonly used formula $C = 4\kappa^2/\gamma_{R1}\gamma_{FM}$ [39,68].
[85] R. Verba, I. Lisenkov, I. Krivorotov, V. Tiberkevich, A. Slavin, Nonreciprocal surface acoustic waves in multilayers with magnetoelastic and interfacial Dzyaloshinskii-Moriya interactions, Phys. Rev. Appl. 9 (2018), 064014, https://doi.org/10.1103/PhysRevApplied.9.064014.
[86] M. Küß, M. Heigl, L. Flacke, A. Hörner, M. Weiler, M. Albrecht, A. Wixforth, Nonreciprocal Dzyaloshinskii–Moriya magnetoacoustic waves, Phys. Rev. Lett. 125 (2020), 217203, https://doi.org/10.1103/PhysRevLett.125.217203.
[87] A. Hernández-Mínguez, F. Macià, J.M. Hernàndez, J. Herfort, P.V. Santos, Large nonreciprocal propagation of surface acoustic waves in epitaxial ferromagnetic/semiconductor hybrid structures, Phys. Rev. Appl. 13 (2020), 044018, https://doi.org/10.1103/PhysRevApplied.13.044018.
[88] M. Xu, K. Yamamoto, J. Puebla, K. Baumgaertl, B. Rana, K. Miura, H. Takahashi, D. Grundler, S. Maekawa, Y. Otani, Nonreciprocal surface acoustic wave propagation via magneto-rotation coupling, Sci. Adv. 6 (32) (2020) eabb1724, https://doi.org/10.1126/sciadv.abb1724.
[89] B. Casals, N. Statuto, M. Foerster, A. Hernández-Mínguez, R. Cichelero, P. Manshausen, A. Mandziak, L. Aballe, J.M. Hernàndez, F. Macià, Generation and imaging of magnetoacoustic waves over millimeter distances, Phys. Rev. Lett. 124 (2020), 137202, https://doi.org/10.1103/PhysRevLett.124.137202.
[90] D.D. Yaremkevich, A.V. Scherbakov, S.M. Kukhtaruk, T.L. Linnik, N.E. Khokhlov, F. Godejohann, O.A. Dyatlova, A. Nadzeyka, D.P. Pattnaik, M. Wang, S. Roy, R. P. Campion, A.W. Rushforth, V.E. Gusev, A.V. Akimov, M. Bayer, Protected long-distance guiding of hypersound underneath a nano-corrugated surface, ACS Nano 15 (3) (2021) 4802–4810, https://doi.org/10.1021/acsnano.0c09475.
[91] N.E. Glass, A.A. Maradudin, Leaky surface-elastic waves on both flat and strongly corrugated surfaces for isotropic, nondissipative media, J. Appl. Phys. 54 (2) (1983) 796–805, https://doi.org/10.1063/1.332038.
[92] N.E. Khokhlov, P.I. Gerevenkov, L.A. Shelukhin, A.V. Azovtsev, N.A. Pertsev, M. Wang, A.W. Rushforth, A.V. Scherbakov, A.M. Kalashnikova, Optical excitation of propagating magnetostatic waves in an epitaxial galfenol film by ultrafast magnetic anisotropy change, Phys. Rev. Appl. 12 (2019), 044044, https://doi.org/10.1103/PhysRevApplied.12.044044.
[93] M. Weiler, H. Huebl, F.S. Goerg, F.D. Czeschka, R. Gross, S.T.B. Goennenwein, Spin pumping with coherent elastic waves, Phys. Rev. Lett. 108 (2012), 176601, https://doi.org/10.1103/PhysRevLett.108.176601.
[94] M. Jäckl, V.I. Belotelov, I.A. Akimov, I.V. Savochkin, D.R. Yakovlev, A.K. Zvezdin, M. Bayer, Magnon accumulation by clocked laser excitation as source of long-range spin waves in transparent magnetic films, Phys. Rev. X 7 (2017), 021009, https://doi.org/10.1103/PhysRevX.7.021009.
[95] M. Kobecki, A.V. Scherbakov, T.L. Linnik, S.M. Kukhtaruk, V.E. Gusev, D. Pattnaik, I.A. Akimov, A.W. Rushforth, A.V. Akimov, M. Bayer, Resonant thermal energy transfer to magnons in a ferromagnetic nanolayer, Nat. Commun. 11 (2020) 4130, https://doi.org/10.1038/s41467-020-17635-1.
[96] M. Kobecki, G. Tandoi, E. Di Gaetano, M. Sorel, A.V. Scherbakov, T. Czerniuk, C. Schneider, M. Kamp, S. Höfling, A.V. Akimov, M. Bayer, Picosecond ultrasonics with miniaturized semiconductor lasers, Ultrasonics 106 (2020), 106150, https://doi.org/10.1016/j.ultras.2020.106150.
[97] D.D. Yaremkevich, A.V. Scherbakov, L. De Clerk, S.M. Kukhtaruk, A. Nadzeyka, R. Campion, A.W. Rushforth, S. Savel'ev, A.G. Balanov, M. Bayer, On-chip phonon-magnon reservoir for neuromorphic computing, https://doi.org/10.21203/rs.3.rs-2789677/v1.

Dr. Alexey V. Scherbakov is a senior researcher in the Experimentelle Physik 2 at the Technische Universität Dortmund (Germany). In 1997 he graduated St. Petersburg Electrotechnical University with Master degree in Optoelectronics and received his PhD degree in 2003 in the Ioffe Institute of the Russian Academy of Sciences (St. Petersburg, Russia). In 2000 – 2017, before joining E2 at TU Dortmund, Dr. Scherbakov had been working as a researcher in the Solid State Spectroscopy Laboratory and the Laboratory of Physics of Ferroics of the Ioffe Institute and as a guest researcher at the Julius-Maximilians-Universität Würzburg (Germany). His research interests are in the fields of ultrafast acoustics, ultrafast optical and magnetooptical spectroscopy with the focus on magnon-phonon and exciton-phonon interaction.

Dr. Tetiana L. Linnik is a senior researcher in the Department of Theoretical Physics of the Lashkaryov Institute of Semiconductor Physics (Kyiv, Ukraine). She obtained degree of Master of Science (in Physics) at the Kyiv State University in 1994 and joined the Lashkaryov Institute, where she received her PhD degree in 2002. Her research interests are theory of electron-phonon and magnon-phonon interaction and ultrafast lattice dynamics at the nanoscale at the intersection of theory and experiment. Since 2022 Dr. Linnik is a guest fellow of the Technische Universität Dortmund (Germany) in the frame of the Philipp Schwartz Initiative supported by Alexander von Humboldt Foundation.

Dr. Serhii Kukhtaruk is a senior researcher in the Department of Theoretical Physics of the Lashkaryov Institute of Semiconductor Physics (Kyiv, Ukraine). He graduated the Taras Shevchenko National University of Kyiv in 2007 with Master degree in theoretical physics. He start his work in the Lashkaryov Institute in 2007, where he received PhD degree in 2013. In 2017 – 2021 Dr. Kukhtaruk was a member of the research group in TU Dortmund and took part in the development of miniaturized microwave magnetic field generators for magnetic resonance imaging. The research interest of Dr. Kukhtaruk are collective excitations in condensed matter including phonons, magnons, plasmons and polaritons, and in-detail numerical modelling of the dynamical processes of these excitations.

Prof. Dr. Dmitri Yakovlev is APL Professor in the 2nd Chair of Experimental Physics (E2) at the Technische Universität Dortmund (Germany). He received his Master diploma in Physics in 1985 in the State Polytechnical University (St. Petersburg, Russia) and his PhD degree in 1988 in the Ioffe Institute of the Russian Academy of Sciences (St. Petersburg, Russia) where he worked as a junior researcher up to 1990. In 1990–1991 he was an Alexander-von-Humboldt Fellow at the Julius-Maximilians-Universität Würzburg (Germany) and continued his research work in Würzburg as a PostDoc and a research fellow up to 2002. In 2002 he joined the Experimentelle Physik 2 (E2) at the Technische Universität Dortmund. His research interests are in experimental study of exciton and spin physics of semiconductor nanostructures.

Dr. Achim Nadzeyka is senior staff application engineer in Raith GmbH (Dortmund, Germany). He graduated the Ruhr Universität in Bochum and received his Master degree in Physics in 1996. In 1996 – 2002 he worked as a research associate in the Department of Experimental Physics at the Ruhr University and studied the generation of highly charged ions in electron cyclotron resonance ion sources. He received his PhD degree in 2002 and joined Raith GmbH as an application scientists. The research interests of Dr. Nadzeyka are nanofabrication, lithography and microscopy using focused ion beam technology.

Dr. Andrew Rushforth is an associate professor of the School of Physics and Astronomy at the University of Nottingham (Nottingham, UK). He graduated the University of Leeds (1993) and received his PhD degree in Physics at the University of Nottingham in 2001. In 2001 – 2004 Dr. Rushforth was a research associate in the Cavendish Laboratory at the University of Cambridge and then joined the Nottingham University. The research interests of Dr. Rushforth include investigating novel magnetic materials, such as magnetostrictive alloys and antiferromagnetic compounds, and development magnetic nanodevices. The interaction of magnetic excitations and phonons as well as control of magnetic properties by strain are currently a focus of his research.

Prof. Dr. Andrey Akimov is a principal researcher in the School of Physics and Astronomy at the University of Nottingham (UK). He graduated the State Polytechnical University in St. Petersburg (Russia) in 1976, received PhD (1983) and Doctor of Sciences (1994) degrees in physics in Ioffe Institute of the Russian Academy of Sciences (St. Petersburg, Russia) where he carried out his research in the Laboratory of Solid State Spectroscopy in 1977 – 2007. In 1998–2006 he held the position of professor and head of department in the Engineering and Economic University in St. Petersburg. He had a position of Merkator Professor in TU Dortmund in 2004–2005 and received Alexander von Humboldt Research Award in 2013. In 2007 Prof. Akimov joined the University of Nottingham. His present research interests are related to phonon physics in a wide range of materials and devices, exciton-phonon interaction, phonon lasing and phonon nanoscopy.

Prof. Dr. Manfred Bayer is a Full Professor at the Technische Universität Dortmund (Germany). Since 2020 he is also the President of the University. He graduated the Julius-Maximilians-Universität Würzburg (Germany) in 1992 with Master diploma in Physics and received there his PhD degree in Physics in 1997. In 1997 – 2002 he was a research associate in the Technische Physik at the University of Würzburg, where he received the "Walter-Schottky-Award" for young scientists. In 2002 Prof. Bayer became head of the Experimentelle Physik 2 at TU Dortmund. His research interests cover various aspects of optical spectroscopy, nuclear and electron magnetic resonance in semiconductor nanostructures, optics of excitons, interaction of coherent phonons with other elementary excitations in solids and many others optical and magnetic phenomena in solids. He is a member of the Elected Board of Referees of the Deutsche Forschunggemeinschaft, Editor of Physical Review B and was also Associate Editor of Physical Review Letters. He is a fellow of the American Physical Society (since 2012) and a Foreign Member of the Russian Academy of Sciences (since 2016).